journal

J. Am. Ceram. Soc., 97 [3] 816–825 (2014)
DOI: 10.1111/jace.12702

Enhanced Multiferroic and Magnetocapacitive Properties of $(1-x)Ba_{0.7}Ca_{0.3}TiO_3$–$xBiFeO_3$ Ceramics

Cai-Xia Li,[‡,§] Bin Yang,[‡,†] Shan-Tao Zhang,[¶] Rui Zhang,[‡] Ye Sun,[‡] Hong-Jun Zhang,[‖] and Wen-Wu Cao[‡,††]

[‡]Department of Physics, Condensed Matter Science and Technology Institute, Harbin Institute of Technology, Harbin 150001, China

[§]Department of Material Physics, School of Applied Sciences, Harbin University of Science and Technology, Harbin 150080, China

[¶]Department of Materials Science and Engineering, National Laboratory of Solid State Microstructures, Nanjing University, Nanjing 210093, China

[‖]Institute for Advanced Ceramics, School of Materials Science and Engineering, Harbin Institute of Technology, Harbin 150001, China

[††]Materials Research Institute, The Pennsylvania State University, University Park, Pennsylvania 16802

The structures, Curie temperature, dielectric relaxor behaviors, ferroelectricity, ferromagnetism, and magnetocapacitance of the $(1-x)Ba_{0.70}Ca_{0.30}TiO_3$–$xBiFeO_3$ [$(1-x)$BCT–xBF, x = 0–0.90] solid solutions have been systematically investigated. The ceramics have coexisted tetragonal (T) and orthorhombic (O) phases when $x \le 0.06$, coexisted pseudocubic (PC) and O phases when $x = 0.065$, coexisted cubic and O phases when $0.07 \le x \le 0.12$, PC phase when $0.21 \le x \le 0.42$, coexisted T and rhombohedral (R) phases when $0.52 \le x \le 0.70$, and R phase when $x \ge 0.75$. Significantly, composition-dependent microstructures and Curie temperature are observed, the average grain size increases from 1.9 μm for $x = 0$, reaches 12.0 μm for $x = 0.67$, and then decreases to 1.3 μm for $x = 0.90$. At room temperature, the ceramics with $x = 0.42$–0.70 show piezoelectric properties and multiferroic behaviors, characterized by the polarization-electric field, polarization current intensity–electric field, and magnetization–magnetic field curves, the composition with $x = 0.67$ has maximum polarization, remnant polarization, maximum magnetization, and remnant magnetization of 15.0 μC/cm^2, 9.1 μC/cm^2, 0.33 emu/g, and 0.14 emu/g, respectively. In addition, the magnetocapacitance is evidenced by the increased relative dielectric constant with increasing the applied magnetic field (H). With $\Delta H = 8$ kOe, the composition with $x = 0.67$ shows the largest values of $(\varepsilon_r(H) - \varepsilon_r(0))/\varepsilon_r(0) = 2.96\%$ at room temperature. The structure–property relationship is discussed intensively.

I. Introduction

Materials that exhibit ferromagnetic and ferroelectric orders simultaneously, termed as "multiferroics," have recently attracted considerable attention.[1–3] The coupling physics between ferromagnetic and ferroelectric orders is expected to produce new properties, such as magnetoelectric, magnetooptic, magnetocapacitive, and other new coupling properties.[3–6] These properties have potential applications in practical electronic devices such as actuators, transducers, sensors, and optical filters.[7,8] From scientific point of view, single-phase multiferroics are appropriate objects to investigate the intrinsic coupling effect between magnetic and electric orders. However, very few single-phase materials exhibit ferroelectric and ferromagnetic properties simultaneously, and most of ferroelectric ferromagnets exhibit rather weak ferromagnetism or antiferromagnetism, where the corresponding magnetocapacitance is almost negligible.[9] It is suggested that most of ferroelectrics are transition-metal oxides,[10] they require empty d orbitals for the off-center displacement of cations, which are responsible for ferroelectricity, whereas the magnetism results from partially filled d orbitals. The difference in the d orbitals required for the ferroelectricity and magnetism makes these two orders mutually exclusive, which explains the rare occurrence of coexisting ferroelectric and ferromagnetic orders.[5] Various methods have been used to synthesize single phase multiferroics. For instance, doping ferroelectric materials with magnetic ions,[11,12] forming solid solutions of ferroelectric materials and ferromagnetic materials,[13,14] etc.

$BiFeO_3$ (BF) is one of the best candidates for multiferroic materials with an antiferromagnetic Néel temperature of 370°C and a high ferroelectric Curie temperature of 830°C,[6] in which the lone electron pair of stereochemically active Bi^{3+} introduces an off-center distortion and thus induces a spontaneous ferroelectric polarization, whereas the superexchange interaction between the Fe^{3+} ions causes G-type antiferromagnetic order.[9] To obtain large magnetocapacitance, large ferroelectric and ferromagnetic ordering parameters could be requested. However, the low resistivity of bulk BF which is mainly caused by the valence fluctuation of Fe ions and the existence of second phases,[7,15,16] makes it difficult to observe the intrinsic ferroelectric nature. Furthermore, the inhomogeneous spatially modulated spiral spin structure with an incommensurate spiral period of ~620 Å of bulk BF results in the cancellation of macroscopic magnetization and prohibits the observation of magnetocapacitance.[17,18.]

Aimed at these problems, considerable efforts have been made to obtain BF-based multiferroic ceramics with increased resistivity and improved magnetic properties. For example, making chemical substitution,[9,10,18] applying high magnetic field,[17] forming solid solutions of BF and other ABO_3 perovskite materials.[13,14,19] Generally, forming solid solutions is an effective way to increase the resistivity and

X. Tan—contributing editor

Manuscript No. 32840. Received March 5, 2013; approved October 7, 2013.
†Author to whom correspondence should be addressed. e-mail: binyang@hit.edu.cn

enhance ferroelectric property. For example, xBiFeO$_3$–(1−x)BaTiO$_3$ (BF–BT) have been intensively studied.[19–21] However, such solid solutions generally show weak magnetic behavior, and in addition, BF–BT solutions with high BF content still show low resistivity. As a result, the magnetocapacitance is not improved significantly.

On the other hand, diphasic materials have been known to possess the potential for performance far beyond those of constituent materials.[22] One of the typical examples is $Ba_{1-x}Ca_xTiO_3$ (BCT100x), which have coexisted ferroelectric T and nonferroelectric O phases when $0.23 \le x \le 0.90$, and show higher electrostrictive strain, higher ferroelectric properties, and higher piezoelectric properties than the single-phase BCT100x with $x < 0.23$ and $x > 0.90$.[22]

Based on the above descriptions, it might be very interesting to prepare and investigate a new solid solution of diphase $Ba_{0.70}Ca_{0.30}TiO_3$ (BCT30) and single-phase BF, the former possesses diphasic T and O phases near the solubility limit ($x = 0.23$),[22] whereas the later possesses R phase at room temperature. It is expected that the introduction of BF can result in coexistence of ferroelectricity and ferromagnetism of BCT30 at room temperature, and coexistence of R and T ferroelectric phases with the additional O phase may be helpful for improving resistivity. Thus, this system may have enhanced multiferroic properties and probably observable magnetocapacitance. In this study, we investigate the structures, ferroelectric, ferromagnetic, and magnetocapacitive properties of the (1−x)$Ba_{0.70}Ca_{0.30}TiO_3$–xBiFeO$_3$ [(1−x)BCT–xBF, x = 0–0.90] ceramics. Composition-dependent ferroelectric, ferromagnetic, and magnetocapacitive properties have been discussed based on the composition-dependent structure.

II. Experimental Procedure

(1−x)BCT–xBF (x = 0, 0.07, 0.08, 0.09, 0.12, 0.21, 0.30, 0.35, 0.42, 0.52, 0.67, 0.70, 0.75, 0.80, and 0.90) ceramics were prepared by the conventional sintering method. Dried raw materials of $BaCO_3$ (99.0%), $CaCO_3$ (99.0%), TiO_2 (99.0%), Bi_2O_3 (99.9%), and Fe_2O_3 (99.99%) were mixed according to the stoichiometric formula and ball-milled in alcohol for 24 h, calcined at 850°C for 3 h, and then ball-milled again for 24 h. Disks with a diameter of 13 mm and a thickness of 0.5–1 mm were pressed under 100 MPa using 8% polyvinyl alcohol binder. The binder was burnt out at 550°C for 2 h. Sintering was carried out between 1000°C and 1250°C in air for 1 h, sintering temperatures decreased with increasing BF content, followed by a furnace cooling. All the disks were embedded in the corresponding powder to reduce the evaporation of Bi during sintering. All the samples had relative densities (determined by the Archimedes method) higher than 95%.

The crystal structures of the ceramics were examined an X-ray diffractometer (XRD, D/Max 2400, Rigaku, Tokyo, Japan) using Cu$K\alpha$ radiation. The microstructures were observed by a scanning electron microscope (SEM, Quanta 200 FEG; FEI Co., Hillsboro, OR). For electrical measurements, both circular surfaces of the samples were covered with a thin layer of silver paste and fired at 600°C for 30 min. Dielectric properties were measured using an Agilent E4980A LCR meter (Agilent Technologies, Santa Clara, CA) in the temperature range 30°C–500°C at different frequencies between 1 and 100 kHz. The room temperature ferroelectric hysteresis loops and the polarization current intensity–electric field (j–E) curves were measured at 1 Hz by precision premier II (Radiant Technology, Albuquerque, NM). For piezoelectric measurement, the samples were poled with the electric field of 20–25 kV/cm in a silicone oil bath. The piezoelectric constant d_{33} was measured using a quasi-static d_{33} meter (Institute of Acoustics, Chinese Academy of Sciences, Beijing, China). The magnetization–magnetic field curves of (1−x)BCT–xBF powder samples were achieved at room temperature using a vibrating sample magnetometer (VSM7300, Lakeshore Cryotronics Inc., Westerville, OH). The relative

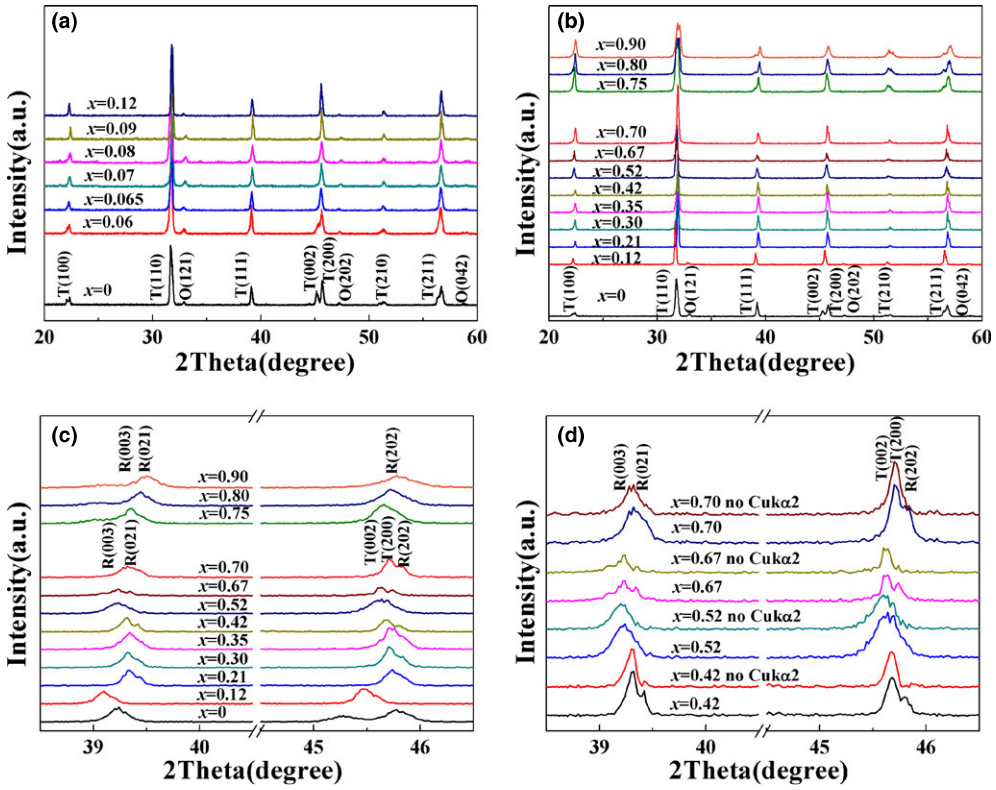

Fig. 1. (a) XRD patterns of (1−x)BCT–xBF ceramics with x = 0–0.12, (b) XRD patterns of (1−x)BCT–xBF ceramics with x = 0–0.90, (c) Expanded view of XRD patterns of (1−x)BCT–xBF ceramics with x = 0–0.90, (d) XRD patterns of (1−x)BCT–xBF ceramics with x = 0.42, 0.52, 0.67, and 0.70 with and without Cu$K\alpha_2$ contribution.

dielectric constant with different applied magnetic fields was measured using E4980A LCR meter (Agilent Technologies) at room temperature.

III. Results and Discussion

Figures 1(a) and (b) show XRD patterns of the $(1-x)$BCT–xBF ceramics with $x = 0$–0.12 and $x = 0$–0.90, respectively. It indicates that series of continuous solid solutions of BCT and BF are formed, and all the ceramics have high-purity perovskite structures without any detectable impurity phases. Further detailed XRD analyses in the 2θ range from 38.5° to 46.5° are shown in Fig. 1(c). It is found that the compositions have diphasic T and O phases when $x \leq 0.06$,[23] characterized by the (002)/(200) splitting peaks near $2\theta \sim 45°$,[24] and the O diffraction peaks. The ceramics with $x = 0.065$ have coexisted PC and O phases, which is consistent with previous reports.[22,23,25] The ceramics have coexisted cubic (C) and O phases when $0.07 \leq x \leq 0.12$. For $x = 0.21$–0.35, the peaks corresponding to O phase disappear and no peak splitting are observable, indicating their PC structure characteristics. XRD patterns of the ceramics with $x = 0.42$, 0.52, 0.67, and 0.70 with and without the contribution of Cu$K\alpha_2$ are supplied simultaneously in Fig. 1(d). It is found that the peak splitting near $2\theta \sim 39.2°$ and 45° disappear in the XRD patterns without the contribution of Cu$K\alpha_2$ of the ceramics with $x = 0.42$, indicating its PC structure characteristic. With x increases, the T(111) and T(200) peaks tend to split and the splitting becomes apparent. The splitting peaks near $2\theta \sim 39.2°$ may be ascribed to the appearance of R phase as pure rhombohedral BF has (003)/(021) peaks near $2\theta \sim 39.2°$ and (202) peak near $2\theta \sim 45.5°$,[8] the distinct peak splitting near $2\theta \sim 45°$ corresponding to T(002)/T(200) and R(202) indicates that T and R phases coexist in the ceramics with $x = 0.52$–0.70. For $x \geq 0.75$, the diffractions peaks corresponding to T phase are not observable, indicating their R structure characteristics, which is in agreement with the R structure characteristics of $(1-x)$BT–xBF ceramics with $x > 0.70$.[26]

All the ceramics show dense microstructures, Fig. 2 shows the typical SEM micrographs of the $(1-x)$BCT–xBF ceramics calcined at 850°C for 3 h and sintered for 1 h with (a) $x = 0.12$ at 1180°C, (b) $x = 0.21$ at 1180°C, (c) $x = 0.35$ at 1160°C, (d) $x = 0.42$ at 1120°C, (e) $x = 0.52$ at 1100°C, (f) $x = 0.67$ at 1040°C, (g) $x = 0.70$ at 1000°C, (h) $x = 0.75$ at 1000°C, (i) $x = 0.80$ at 1000°C, and (j) $x = 0.90$ at 1000°C. It can be seen that with increasing BF content, the average grain size increases significantly from 1.9 μm for $x = 0$, reaches the maximum of 12.0 μm for $x = 0.67$ and then decreases to 1.3 μm for $x = 0.90$, which is consistent with the ferroelectric properties reported later.

Figures 3(a)–(d) show the temperature dependence of the relative dielectric constant (ε_r) measured at different frequencies for the ceramics with $x = 0.42$, 0.52, 0.67, and 0.70, respectively. It is found that the temperature corresponding to the maximum relative dielectric constant (T_m) is frequency dependent and shifts to higher temperature with increasing frequency. The diffuse phase transition and frequency dispersion indicate the relaxor behaviors of the ceramics with $x = 0.42$–0.70. To further analyze the relaxation characters of the $(1-x)$BCT–xBF ceramics, the modified empirical expression proposed by Uchino and Nomura[27] is employed as follows:

$$\frac{1}{\varepsilon_r} - \frac{1}{\varepsilon_{rm}} = \frac{(T - T_m)^\gamma}{C} \quad (1)$$

where γ and C are constants and the γ value is between 1 and 2. For the normal ferroelectrics, $\gamma = 1$ and the ε_r above the Curie point obeys the Curie–Weis law. While for the ideal relaxor ferroelectrics, $\gamma = 2$ and the ε_r deviates from the Curie–Weis law above the T_m.[27] The plots of $\ln(1/\varepsilon_r - 1/\varepsilon_{rm})$ versus $\ln(T - T_m)$ and the fitting curves are given in Fig. 3. The γ values are determined from the slope of the fitting curves. It can be seen that the parameter γ increases with increasing BF content and reaches the maximum of 1.852 for $x = 0.67$, indicating the enhanced typical relaxor behavior. It is suggested that the A-sites Bi^{3+} substitution together with the additional B-sites Fe^{3+} substitution create charge imbalance in $(1-x)$BCT–xBF ceramics, which should be compensated by either A-site or B-site cation vacancies, or by electrons.[28] These factors may disrupt the long-range ordering of the BCT ceramics, which are responsible for the ferro-

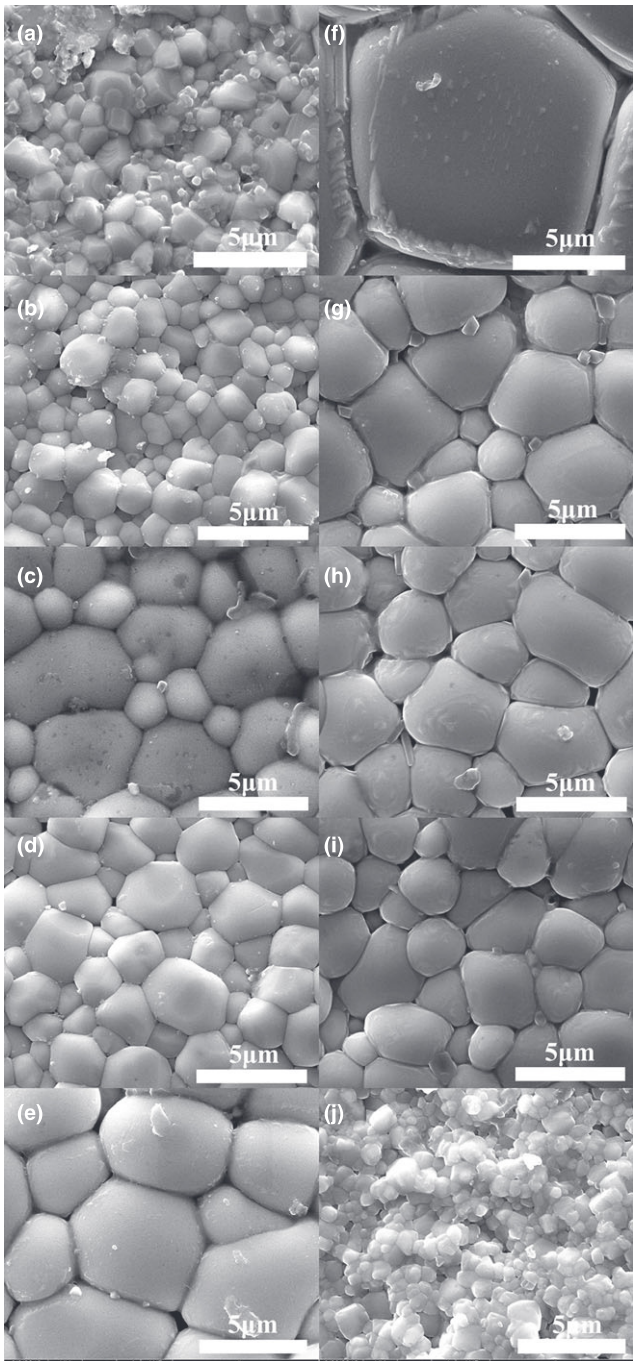

Fig. 2. SEM micrographs of $(1-x)$BCT–xBF ceramics sintered for 1 h (a) $x = 0.12$ at 1180°C, (b) $x = 0.21$ at 1180°C, (c) $x = 0.35$ at 1160°C, (d) $x = 0.42$ at 1120°C, (e) $x = 0.52$ at 1100°C, (f) $x = 0.67$ at 1040°C, (g) $x = 0.70$ at 1000°C, (h) $x = 0.75$ at 1000°C, (i) $x = 0.80$ at 1000°C, (j) $x = 0.90$ at 1000°C.

electric relaxor behavior. With increasing BF content, γ decreased gradually to 1.816 when $x = 0.70$, indicating the weakened relaxor behavior which may be partially related to the increased inner stress.[29]

The T_m of the $(1-x)$BCT–xBF ceramics as a function of BF content measured at different frequencies are plotted in Fig. 4(a). As can be seen, T_m shows evident frequency dispersion characteristics. It is suggested that the degree of relaxor behavior could be estimated by the empirical parameter ΔT_{relax} defined as follows:

$$\Delta T_{\text{relax}} = T_{\text{m}}(100\ \text{kHz}) - T_{\text{m}}(1\ \text{kHz}) \quad (2)$$

where T_m(100 kHz) and T_m(1 kHz) are the temperatures corresponding to the dielectric constant maximum at frequencies of 100 and 1 kHz, respectively. Figure 4(b) shows the ΔT_{relax} of the $(1-x)$BCT–xBF ceramics as a function of BF content. It is found that with x increases, the ΔT_{relax} increases and reaches the maximum of 99 for $x = 0.67$, and then decreases, indicating that the degree of relaxor behavior is dependent on BF content in the $(1-x)$BCT–xBF ceramics, consistent with our previous report.[23]

With x increases, T_m decreases and reaches the minimum of 3°C at 10 kHz for $x = 0.07$, then increases and reaches the maximum of 361°C at 10 kHz for $x = 0.67$, and finally T_m decreases to 268°C for $x = 0.90$, as shown in Fig. 4(a). For $x \le 0.07$, the decrease in T_m may be ascribed to decreased internal stress in increased grain size of T phase and the local random electric fields caused by the cosubstitution of A-site Bi^{3+} and B-site Fe^{3+}, which are consistent with our previous report.[23,28] For $x = 0.08$–0.90, the change in T_m may be interpreted based on the stress model.[30] As is known, fine-grained BT-based ceramics have higher inner stress due to the absence of 90° domain walls, and with the grain size increases, the inner stress can be slightly removed by the appearance of repeatedly twined 90° domain walls.[31] In the cases of our $(1-x)$BCT–xBF system, the increase in T_m with increasing x when $0.08 \le x \le 0.67$ may be partially related to the decreased inner stress with increasing the grain size, whereas T_m shifts to lower temperature with increasing x when $0.70 \le x \le 0.90$, which may be ascribed to the increased

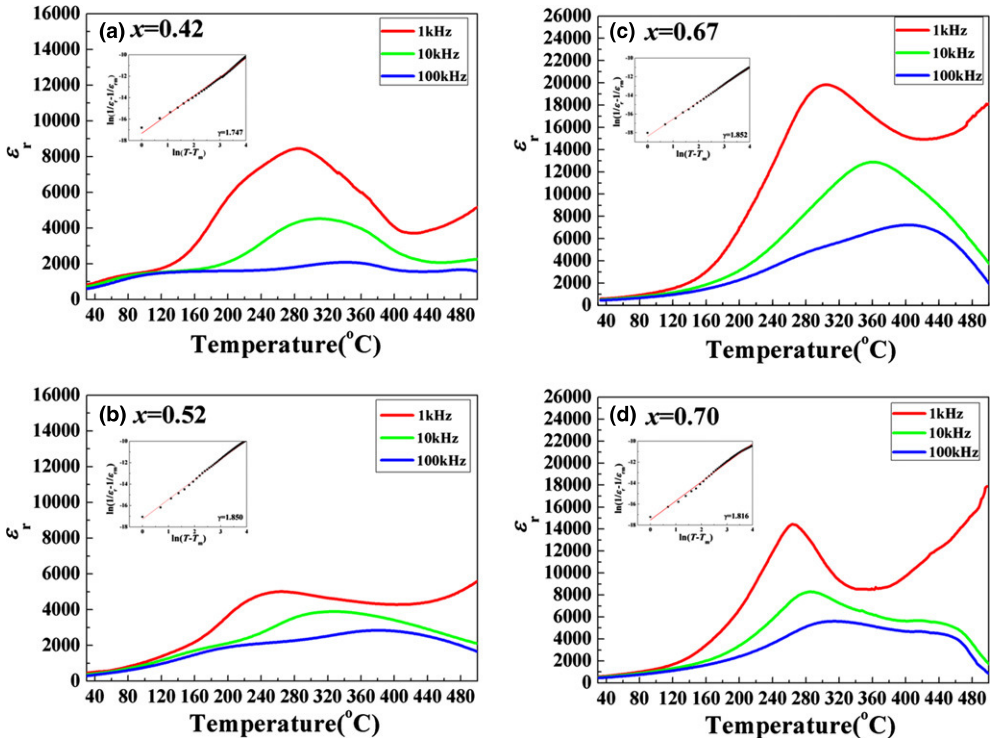

Fig. 3. Temperature-dependent dielectric properties of $(1-x)$BCT–xBF ceramics (a) $x = 0.42$, (b) $x = 0.52$, (c) $x = 0.67$ and (d) $x = 0.70$ (Insets are the corresponding curves of ln $(1/\varepsilon_r - 1/\varepsilon_{rm})$ against ln $(T - T_m)$ at 10 kHz).

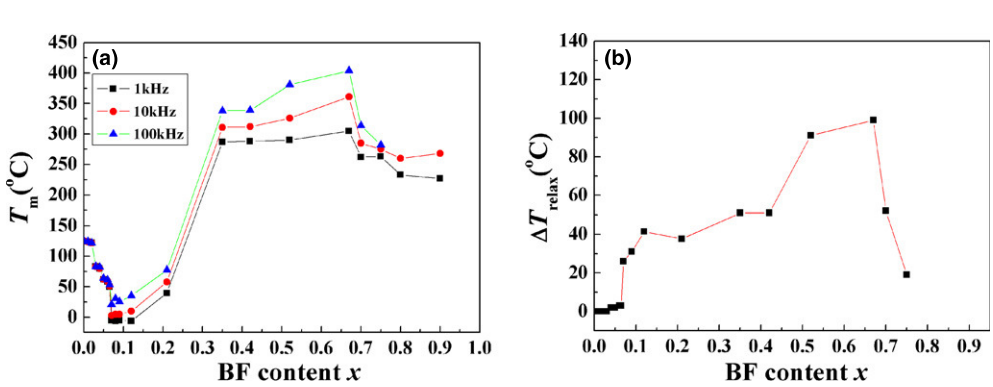

Fig. 4. (a) T_m of $(1-x)$BCT–xBF ceramics as a function of BF content at different frequencies, (b) the ΔT_{relax} of $(1-x)$BCT–xBF ceramics as a function of BF content.

inner stress with reducing grain size of the ceramics.[30,31] The exact origin of the changed T_m of the $(1-x)$BCT–xBF solid solutions is still unclear and is left for future studies.

Figures 5(a)–(j) plot the room-temperature polarization–electric field (P–E) hysteresis loops of the $(1-x)$BCT–xBF ceramics (x = 0.12–0.90). The shown loops, which are dominated by the contributions of leakage currents, domain

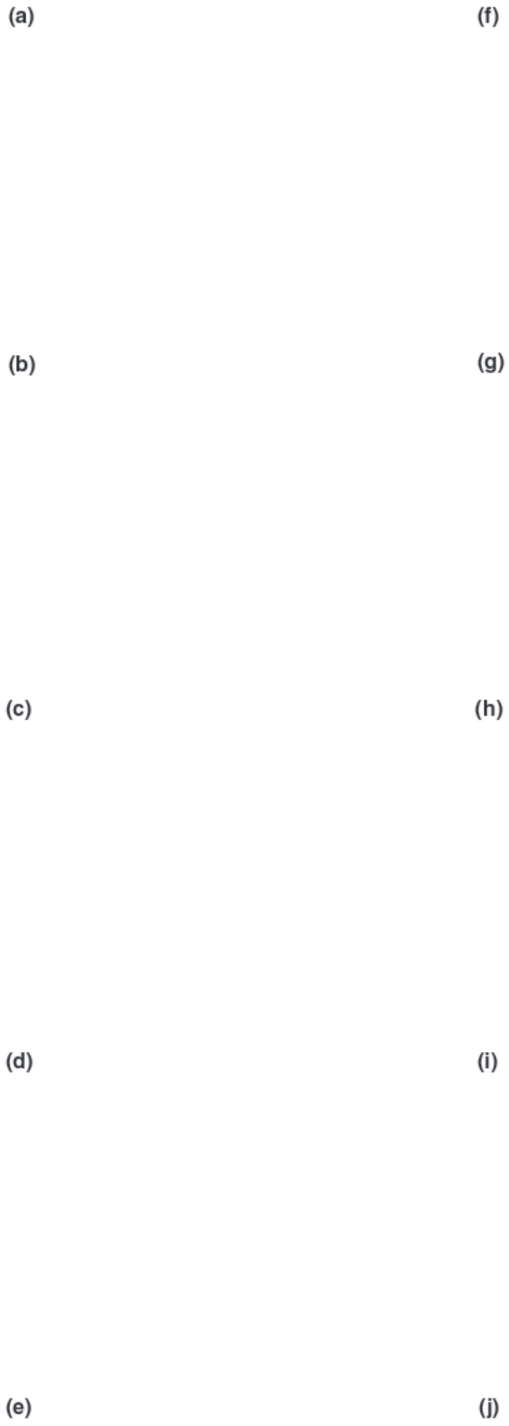

Fig. 5. P–E hysteresis loops of $(1-x)$BCT–xBF (x = 0.12–0.90) ceramics measured at room temperature.

switching, and linear capacitance, were measured with different applied electric fields (70 kV/cm for compositions with $x = 0.12$–0.70, whereas 20 kV/cm for $x = 0.75$–0.90). The "loops" of the compositions with $x = 0.12$, 0.21, 0.35, and 0.42 are very slim, whereas the loops of the compositions with $x = 0.52$, 0.67, and 0.70 have the saturation tendency. For the ceramics with $x = 0.75$, 0.80, and 0.90, the low resistivity makes the ferroelectric measurement difficult, and their loops show ellipse-like rounded features. The low resistivity may be ascribed to the mix valance of Fe ions and O vacancies, which is responsible for large leakage current and unfavorable for the observation of saturated polarization.[32]

The reorientation of polarization could not be easily detected from the *P–E* responses. Although the presence of a *P–E* hysteresis loop is always regarded as an evidence of ferroelectricity, the hysteretic behavior may also occur in nonferroelectric systems.[33,34] For instance, many lossy dielectrics exhibit closed cigar-shaped *P–E* hysteresis loops which have nonferroelectric properties.[34,35] Therefore, it is essential to distinguish whether the materials studied have true ferroelectric properties. Wang *et al.*[36] and Yan *et al.*[37] provide an instructive method to measure the ferroelectric properties by distinguishing the contributions of linear capacitance, electric conductivity, and domain switching in current–electric field loops and *P–E* hysteresis loops. To observe the reorientation of polarization, the polarization current intensity–electric field (*j–E*) loops of the ceramics with $x = 0.42$, 0.52, 0.67, 0.70 were measured at 1 Hz and are shown in Figs. 6(a)–(d). It is found that the *j–E* loop of the composition with $x = 0.42$ is dominated by the contribution of linear capacitance, and the polarization current intensity of the ceramics with $x = 0.52$, 0.67, and 0.70 show very broad and flat peaks at the nonergodic state, indicating the ferroelectric domains reversal and relaxor ferroelectric behaviors for the ceramics with $x = 0.52$–0.70.[36,37] As x increases from 0.42 to 0.70, the remnant polarization (P_r) shows a drastic increase and reaches the maximum of 9.1 $\mu C/cm^2$ at $x = 0.67$, indicating the enhanced ferroelectricity. The increase in measured "P_r" could be mainly due to the contribution of leakage currents. It is suggested that electrical hysteresis measurement requires metal contacts and permits charge injection and real current. The larger leakage current in the ceramics with $x = 0.67$ may result from mixed valence of the magnetic Fe ions, oxygen vacancies, or both. On the other hand, the significantly increased grain size (as shown in Fig. 2) is an extrinsic effect and positive for the enhanced ferroelectricity of the ceramics with $x = 0.67$, as it is suggested that small grain size means large amount of grain boundary, and grain boundary will leads to polarization discontinuity between grains and hence decreased polarization.[38] Moreover, with increasing BF content, Bi^{3+} occupies the A-site, and Fe^{3+} occupies the B-site, cation vacancies on the A- site or B-site, oxygen vacancies, or electrons will appear to maintain the charge neutrality, which can pin the domain wall motion, decrease resistivity, suppress ferroelectric property, and the observation of saturated polarization. So, it is difficult to observe the ferroelectric properties of the ceramics with $x \geq 0.75$.

The d_{33} of the ceramics with $x = 0.42$, 0.52, 0.67, and 0.70 are 13, 15, 20, and 16 pC/N, respectively. The poor piezoelectric property may be ascribed to the large leakage currents as shown in Fig. 6 which makes the electrical poling of the ceramics under DC electric field difficult.

The room-temperature magnetization–magnetic field (*M–H*) curves of the $(1-x)$BCT–xBF ceramics ($x = 0.35$, 0.42, 0.52, 0.67, 0.70, 0.75, 0.80, and 0.90) were measured with a maximum magnetic field of 10 kOe, as shown in Figs. 7(a)–(h). The composition with $x = 0.35$ shows "S" type *M–H* curve indicating the superparamagnetic. The superparamagnetic behavior of this composition is similar to that of 1% Fe-doped $BaTiO_3$ ceramic and single crystal.[39] Actually at low substituting/doping level of BF such as $x = 0.35$, the average distance between neighboring magnetic Fe ions is so large that they are not be able to establish magnetic exchange interactions.[39] A further increase in the magnetization value and *M–H* loops are observed for the $(1-x)$ BCT–xBF ceramics with $x = 0.42$–0.90, indicating typical ferromagnetic behaviors at room temperature. The origin of ferromagnetism can be ascribed to two possible aspects:

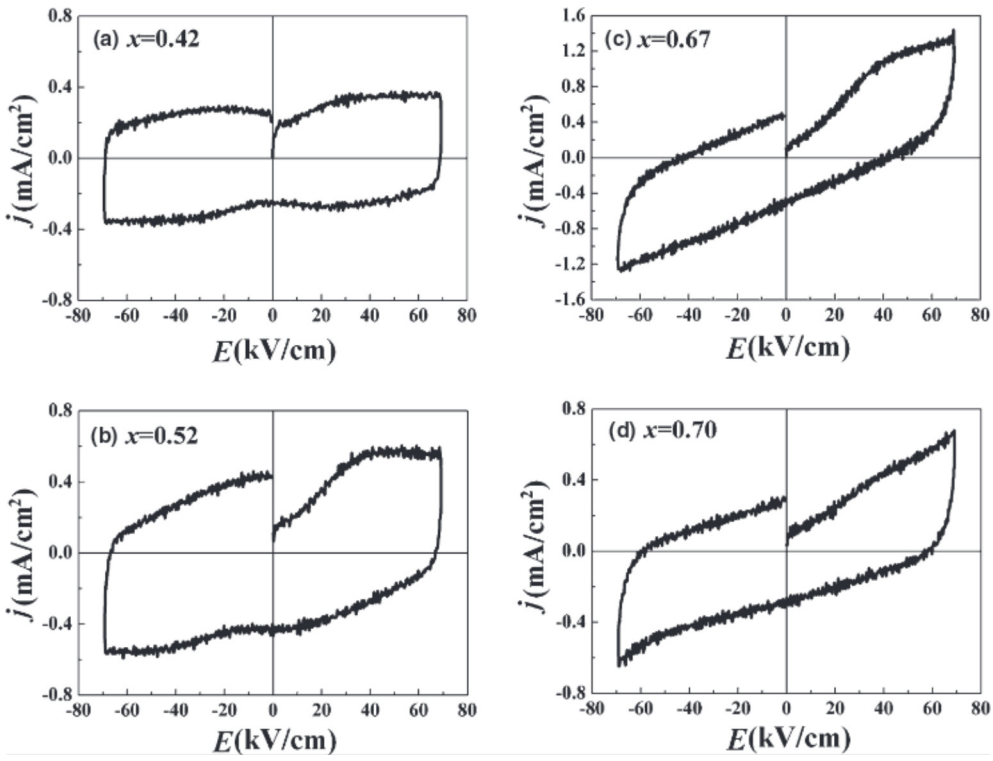

Fig. 6. Room temperature polarization current intensity–electric filed loops of the $(1-x)$BCT–xBF ceramics measured at 1 Hz (a) $x = 0.42$, (b) $x = 0.52$, (c) $x = 0.67$ and (d) $x = 0.70$.

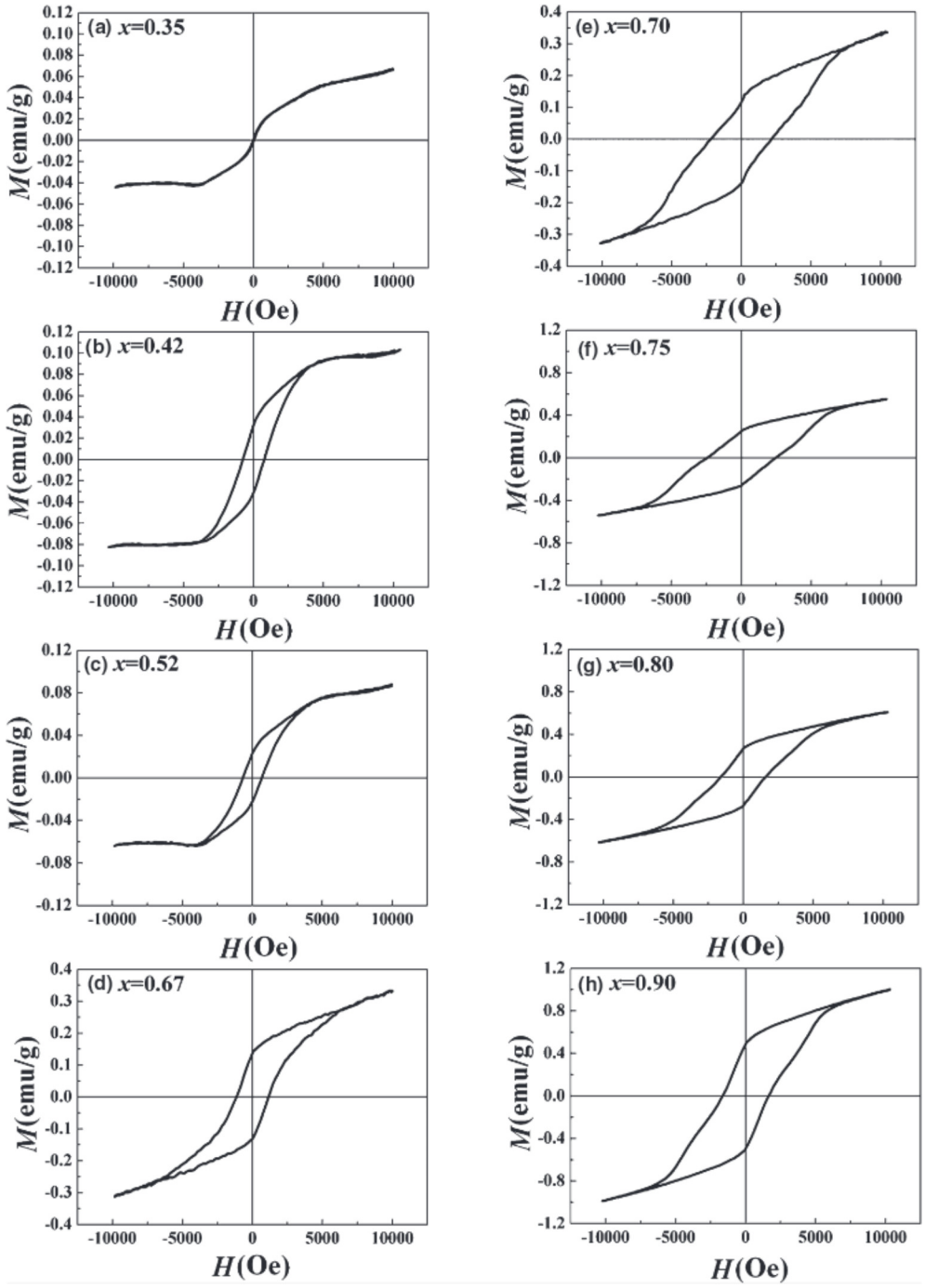

Fig. 7. Magnetic hysteresis loops of $(1-x)$BCT–xBF ceramics measured at room temperature (x = 0.35–0.90).

First, BF possesses a R distorted perovskite structure, allowing a weak ferromagnetic ordering due to canting of spins. With increasing BF content, the bond angle of Fe–O–Fe may be changed, resulting in the magnetization of $(1-x)$BCT–xBF ceramics.[8] On the other hand, Fe^{2+} or oxygen vacancies may appear to compensate the charge imbalance arising from the cosubstitution of Ba^{2+}, Ca^{2+} ions by Bi^{3+}, and Ti^{4+} by Fe^{3+} ions, as evidenced by the decreased resistivity. The statistical distribution of Fe^{3+} and Fe^{2+} may also lead to net magnetization and ferromagnetism.

The maximum magnetization (M_{max}), remnant magnetization (M_r), and coercive field (H_C) as a function of x are plotted in Fig. 8. Generally, the M_{max} and M_r increase with increasing BF content. For the ceramics with $x = 0.67$, $M_{max} = 0.33$ emu/g, $M_r = 0.14$ emu/g. It is suggested that with x increases, a larger amount of Fe^{3+} ions participate in producing ferromagnetism, the average distance between neighboring Fe^{3+} ions decreases, the magnetic exchange interactions between neighboring Fe^{3+} ions enhance, resulting in the enhanced magnetization. H_C increases with increasing x, reaches the maximum of 2.4 kOe at $x = 0.75$, such high coercivity cannot be caused by the pinning of magnetic domain walls alone, the strong coercive force should mainly result from the magnetic anisotropy.[8]

Based on the ferroelectric and magnetic results, enhanced magnetocapacitance of the composition with $x = 0.67$ is expected. The frequency dependence of the room-temperature relative dielectric constant (ε_r) for the $(1-x)$BCT–xBF ceramics (x = 0.42, 0.52, 0.67, 0.70, and 0.75) is shown in Fig. 9(a). It is found that the ε_r values of the ceramics with x = 0.42–0.75 decrease drastically when the frequency increases from 0.04 to 25 kHz, and then gradually become

nearly constant at high frequencies (about 200 kHz). This phenomenon is ascribed to the Maxwell–Wagner-type contribution to ε_r, which is related to the space charge relaxation at the interface.[40] The space charges are suggested to originate from point defects during the quenching process. In the low-frequency range, the space charges are able to follow the frequency of the applied electric field and contribute to ε_r. While with frequency increases, the space charges do not have enough time to build up and undergo relaxation, resulting in the less contribution of space charges to ε_r and decrease in ε_r. The ε_r values of the ceramics with $x = 0.42$, 0.52, 0.67, 0.70, and 0.75 measured at 200 kHz are 612, 488, 412, 270, and 244, respectively, which indicates that the dielectric properties of the $(1-x)$BCT–xBF ceramics ($x = 0.42$–0.75) decrease with increasing BF content. The decreased dielectric properties may be ascribed to the increased density of oxygen vacancies with increasing BF content.

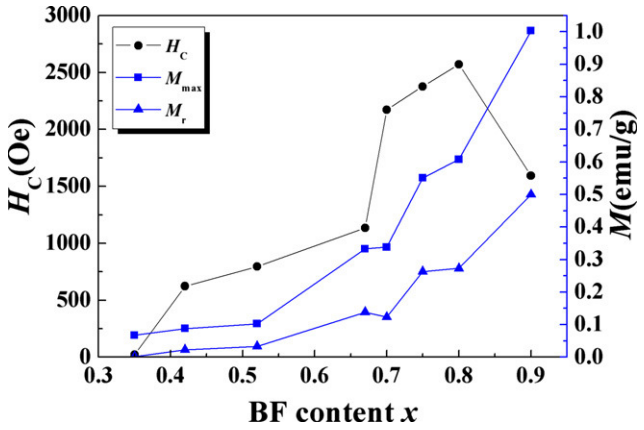

Fig. 8. M_{max}, M_r, and H_C values of $(1-x)$BCT–xBF ceramics as a function of BF content.

To demonstrate the coupling between electric and magnetic polarizations, the variation in the room-temperature ε_r with the DC magnetic field applied along the axis of pellets is measured at different frequencies, as shown in Figs. 9(b)–(f). The magnetocapacitive coefficient is defined by the relative change in the dielectric constant $((\varepsilon_r(H)-\varepsilon_r(0))/\varepsilon_r(0))$.[8,40] With increasing magnetic field, the ε_r and the positive values of magnetocapacitive coefficient depend on both the measuring frequency and the variation in the applied magnetic field. At room temperature with $\Delta H = 10$ kOe, the magnetocapaci-

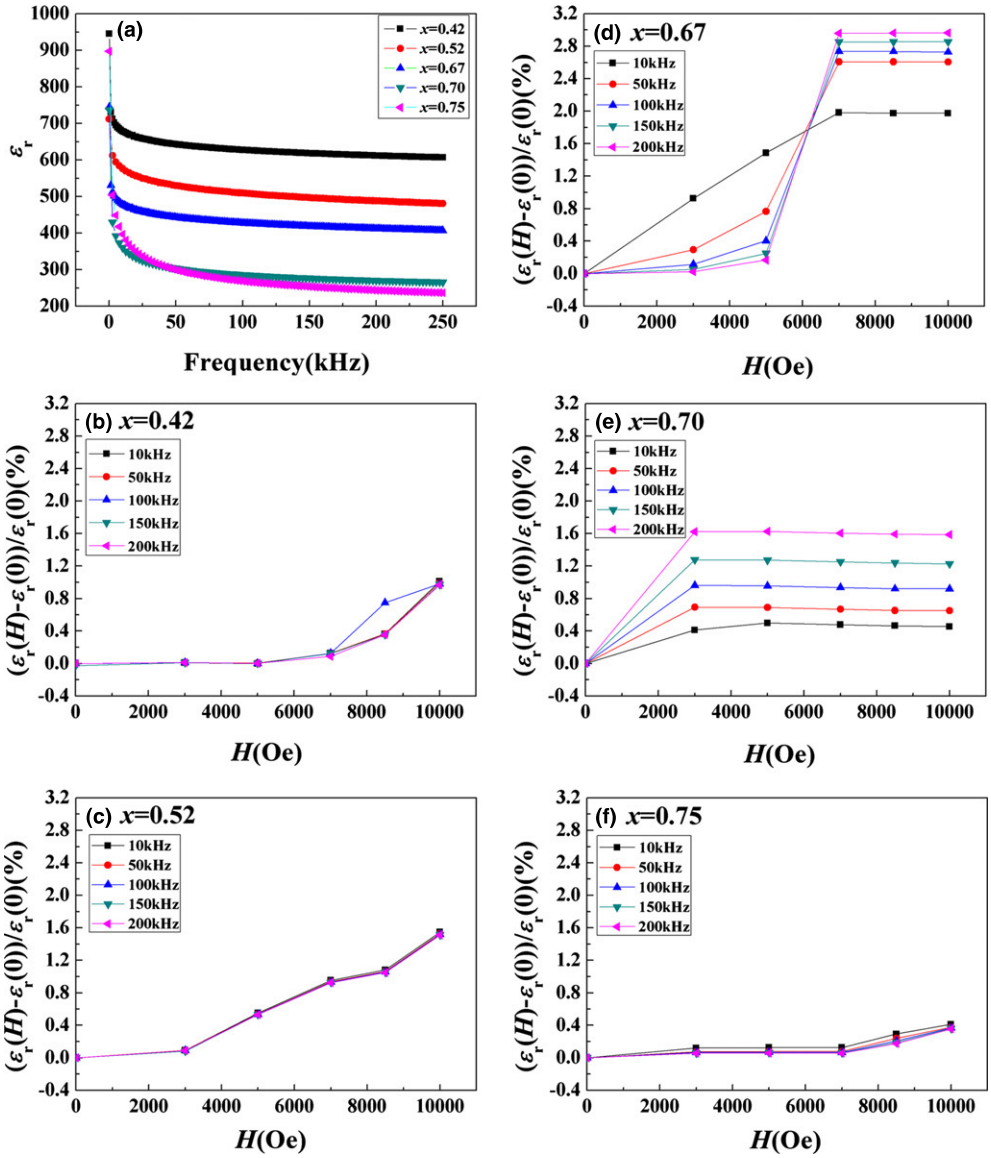

Fig. 9. (a) Frequency—dependent ε_r of $(1-x)$BCT–xBF ceramics with $x = 0.42$–0.75; magnetic field—induced change in ε_r of $(1-x)$BCT–xBF ceramics with (b) $x = 0.42$, (c) $x = 0.52$, (d) $x = 0.67$, (e) $x = 0.70$, (f) $x = 0.75$.

tive coefficient measured at 200 kHz are 1.01%, 1.55%, 2.96%, 1.59%, and 0.41% for $x = 0.42$, 0.52, 0.67, 0.70, and 0.75, respectively. The composition with $x = 0.67$ shows the largest magnetocapacitive coefficient (2.96% at 8 kOe), which is 174% higher than that in the Ba-doped $BiFeO_3$ ceramics (~1.7% at 8 kOe),[8] 384% higher than that in Fe-doped $K_{0.5}Na_{0.5}Nb_{0.95}Ta_{0.05}O_3$ Ceramics,[41] and 190%–720% higher than that of the other compositions of the $(1-x)$BCT–xBF ceramics. The multiferroic materials will be strained when a magnetic field is applied. The coupling between the magnetic and ferroelectric domains will make the strain to induce stress and then generate an electric field on the ferroelectric domains. So the relative dielectric constant will be modified. In addition, the exceptional large grain size of the ceramics with $x = 0.67$ is positive for the enhanced ferroelectricity and enhanced magnetocapacitance.

IV. Conclusions

$(1-x)Ba_{0.70}Ca_{0.30}TiO_3$–$xBiFeO_3$ ($x = 0$–0.90) ceramics have been fabricated and the composition-dependent structure, Curie temperature, dielectric relaxor behaviors, ferroelectricity, ferromagnetism, and magnetocapacitance have been investigated. The compositions have diphasic T and O phases when $x = 0$–0.06, coexisted PC and O phases when $x = 0.065$, coexisted C and O phases when $x = 0.07$–0.12, PC phase when $x = 0.21$–0.42, coexisted T and R phases when $x = 0.52$–0.70, and pure R phase when $x = 0.75$–0.90. Significantly, composition-dependent microstructures and T_m are observed, the average grain size increases from 1.9 μm for $x = 0$, reaches 12.0 μm for $x = 0.67$, and then decreases to 1.3 μm for $x = 0.90$. The most superior multiferroic properties are obtained in the composition with $x = 0.67$ with $P_{max} = 15.0\ \mu C/cm^2$, $P_r = 9.1\ \mu C/cm^2$, $M_{max} = 0.33$ emu/g, and $M_r = 0.14$ emu/g. With $\Delta H = 8$ kOe, this composition shows the largest magnetocapacitive coefficient of 2.96%. These results imply that the $(1-x)Ba_{0.70}Ca_{0.30}TiO_3$–$xBiFeO_3$ may have potential application as multiferroic materials in the future, and it may be helpful for further understanding the intrinsic magnetoelectric interaction and discovering novel high-performance multiferroic materials.

Acknowledgments

This work was supported by the National Science and Technology Support Program (2013BAI03B06), the National Key Basic Research Program of China (973 Program, 2013CB632900), the National Nature Science Foundation of China (10704021, 51102062 and 11174127), the Key Scientific and Technological Project of Harbin (grant no. 2009AA3BS131).

References

[1]W. Eerenstein, N. D. Mathur, and J. F. Scott, "Multiferroic and Magnetoelectric Materials," *Nature (London)*, **442**, 759–65 (2006).

[2]N. Hur, S. Park, P. A. Sharma, J. S. Ahn, S. Guha, and S.-W. Cheong, "Electric Polarization Reversal and Memory in a Multiferroic Material Induced by Magnetic Fields," *Nature (London)*, **429**, 392–5 (2004).

[3]J. Hemberger, P. Lunkenheimer, R. Fichtl, H.-A. Krug von Nidda, V. Tsurkan, and A. Loidl, "Relaxor Ferroelectricity and Colossal Magnetocapacitive Coupling in Ferromagnetic $CdCr_2S_4$," *Nature (London)*, **434**, 364–7 (2005).

[4]C. Ederer and N. A. Spaldin, "Weak Ferromagnetism and Magnetoelectric Coupling in Bismuth Ferrite," *Phys. Rev. B*, **71**, 060401, 4pp (2005).

[5]A. Singh, V. Pandey, R. K. Kotnala, and D. Pandey, "Direct Evidence for Multiferroic Magnetoelectric Coupling in $0.9BiFeO_3$–$0.1BaTiO_3$," *: Phys. Rev. L*, **101**, 247602, 4pp (2008).

[6]T. Kimura, S. Kawamoto, I. Yamada, M. Azuma, M. Takano, and Y. Tokura, "Magnetocapacitance Effect in Multiferroic $BiMnO_3$," *Phys. Rev. B*, **67** [18] 180401, 4pp (2003).

[7]M. M. Kumar, V. R. Palkar, K. Srinivas, and S. V. Suryanarayana, "Ferroelectricity in a Pure $BiFeO_3$ Ceramic," *Appl. Phys. Lett.*, **76**[19], 2674–2766 (2000).

[8]D. H. Wang, W. C. Goh, M. Ning, and C. K. Ong, "Effect of Ba Doping on Magnetic, Ferroelectric, and Magnetoelectric Properties in Multiferroic $BiFeO_3$ at Room Temperature," *Appl. Phys. Lett.*, **88**, 212907, 3pp (2006).

[9]V. A. Khomchenko, M. Kopcewicz, A. M. L. Lopes, Y. G. Pogorelov, J. P. Araujo, J. M. Vieera, and A. L. Kholkin, "Intrinsic Nature of the Magnetization Enhancement in Heterovalently Doped $Bi_{1-x}A_xFeO_3$(A = Ca, Sr, Pb, Ba) Multiferroics," *J. Phys. D: Appl. Phys.*, **41**, 102003, 4pp (2008).

[10]V. A. Khomchenko, D. A. Kiselev, J. M. Viera, and A. L. Kholkin, "Synthesis and Multiferroic Properties of $Bi_{0.8}A_{0.2}FeO_3$(A = Ca, Sr, Pb) Ceramics," *Appl. Phys. Lett.*, **90** [24] 242901, 3pp (2007).

[11]M. P. Singh, W. Prellier, L. Mechin, C. Simon, and B. Raveau, "Correlation Between Structure and Properties in Multiferroic $La_{0.7}Ca_{0.3}MnO_3/BaTiO_3$ Superlattices," *J. Appl. Phys.*, **99** [2] 024105–8 (2006).

[12]F. T. Lin, D. M. Jiang, X. M. Ma, and W. Z. Shi, "Influence of Doping Concentration on Room-Temperature Ferromagnetism for Fe-Doped $BaTiO_3$ Ceramics," *J. Magn. Magn. Mater.*, **320**, 691–4 (2008).

[13]N. G. Wang, J. Cheng, A. Pyatakov, A. K. Zvezdin, J. F. Li, L. E. Cross, and D. Viehland, "Multiferroic Properties of Modified $BiFeO_3$–$PbTiO_3$-Based Ceramics: Random-Field Induced Release of Latent Magnetization and Polarization," *Phys. Rev. B*, **72** [10] 104434, 5pp (2005).

[14]Y. X. Wei, X. T. Wang, J. J. Jia, and X. L. Wang, "Multiferroic and Piezoelectric Properties of $0.65BiFeO_3$–$0.35BaTiO_3$ Ceramic With Pseudo-Cubic Symmetry," *Ceram. Int.*, **38** [4] 3499–502 (2012).

[15]Y. P. Wang, L. Zhou, M. F. Zhang, X. Y. Chen, J. M. Liu, and Z. J. Liu, "Room-Temperature Saturated Ferroelectric Polarization in $BiFeO_3$ Ceramics Synthesized by Rapid Liquid Phase Sintering," *Appl. Phys. Lett.*, **84** [10] 1731–3 (2004).

[16]A. K. Pradhan, K. Zhang, D. Hunter, J. B. Dadson, G. B. Loutts, P. Bhattacharya, R. Katiyar, J. Zhang, and D. J. Sellmyer, "Magnetic and Electrical Properties of Single-Phase Multiferroic $BiFeO_3$," *J. Appl. Phys.*, **97** [9] 093903, 4pp (2005).

[17]B. Ruette, S. Zvyagin, A. P. Pytakov, A. A. Bush, J. F. Li, V. I. Belotelov, A. K. Zvezdin, and D. Viehland, "Magnetic-Field-Induced Phase Transition in $BiFeO_3$ Observed by High-Field Electron Spin Resonance: Cycloidal to Homogeneous Spin Order," *Phys. Rev. B*, **69** [6] 064114, 7pp (2004).

[18]S. T. Zhang, Y. Zhang, M. H. Lu, C. L. Du, Y. F. Chen, Z. G. Liu, Y. Y. Zhu, and N. B. Ming, "Substitution-Induced Phase Transition and Enhanced Multiferroic Properties of $Bi_{1-x}La_xFeO_3$ Ceramics," *Appl. Phys. Lett.*, **88** [16] 162901 (2006).

[19]J. S. Kim, C. I. Cheon, C. H. Lee, and P. W. Jang, "Weak Ferromagnetism in the Ferroelectric $BiFeO_3$–$ReFeO_3$–$BaTiO_3$ Solid Solutions (Re = Dy, La)," *J. Appl. Phys.*, **96** [1] 468–74 (2004).

[20]T. J. Park, G. C. Papaefthymiou, A. J. Viescas, Y. L. Lee, H. J. Zhou, and S. S. Wong, "Composition-Dependent Magnetic Properties of $BiFeO_3$–$BaTiO_3$ Solid Solution Nanostructures," *Phys. Rev. B*, **82** [2] 024431 (2010).

[21]F. R. Gheorghiu, A. Ianculescu, P. Postolache, N. Lupu, M. Dobromir, D. Luca, and L. Mitoseriu, "Preparation and Properties of $(1-x)BiFeO_3$–$XBaTiO_3$ Multiferroic Ceramics," *J. Alloy. Compd.*, **506** [2] 862–7 (2010).

[22]X. S. Wang, H. Yamada, and C. N. Xu, "Large Electrostriction Near The Solubility Limit in $BaTiO_3$–$CaTiO_3$ Ceramics," *Appl. Phys. Lett.*, **86** [2] 022905, 3pp (2005).

[23]C. X. Li, B. Yang, S. T. Zhang, F. M. Wu, and W. W. Cao, "Phase Transition and Electrical Properties of $Ba_{0.7}Ca_{0.3}TiO_3$–$BiFeO_3$ Ceramics," *J. Am. Ceram. Soc.*, **95**, 3901–5 (2012).

[24]A. Ullah, C. W. Ahn, S. Y. Lee, J. S. Kim, and I. W. Kim, "Structure, Ferroelectric Properties, and Electric Field-Induced Large Strain in Lead-Free $Bi_{0.5}(Na, K)_{0.5}TiO_3$–$(Bi_{0.5}La_{0.5})AlO_3$ Piezoelectric Ceramics," *Ceram. Int.*, **38**, 363–8 (2012).

[25]X. S. Wang, H. Yamada, K. Nishikubo, and C. N. Xu, "Electrostrictive Properties of Pr-Doped $BaTiO_3$–$CaTiO_3$ Ceramics," *Jpn. J. Appl. Phys.*, **45**, 813–6 (2006).

[26]M. M. Kuamr, S. Srinvias, and S. V. Suryanarayana, "Structure Property Relations in $BiFeO_3/BaTiO_3$ Solid Solutions," *J. Appl. Phys.*, **87** [2] 855–62 (2000).

[27]K. Uchino and S. Nomura, "Critical Exponents of the Dielectric Constants in Diffused Phase Transition Crystals," *Ferroelectr. Lett. Sect.*, **44**, 55–61 (1982).

[28]S. Mahajan, O. P. Thakur, D. K. Bhattacharya, and K. Sreenivas, "Ferroelectric Relaxor Behaviour and Impedance Spectroscopy of Bi_2O_3-Doped Barium Zirconium Titanate Ceramics," *J. Phys. D Appl. Phys.*, **42**, 065413–22 (2009).

[29]H. Yu, H. X. Liu, H. Hao, L. L. Guo, C. J. Jin, Z. Y. Yu, and M. H. Cao, "Grain Size Dependence of Relaxor Behavior in $CaCu_3Ti_4O_{12}$ Ceramics," *Appl. Phys. Lett.*, **91**, 222911, 3pp (2007).

[30]W. R. Buessem, L. E. Cross, and A. K. Goswami, "Phenomenological Theory of High Permittivity in Fine-Grained Barium Titanate," *J. Am. Ceram. Soc.*, **49**, 33–6 (1966).

[31]J. G. Hao, W. F. Bai, W. Li, and J. W. Zhai, "Correlation Between the Microstructure and Electrical Properties in High-Performance $(Ba_{0.85}Ca_{0.15})(Zr_{0.1}Ti_{0.9})O_3$ Lead-Free Piezoelectric Ceramics," *J. Am. Ceram. Soc.*, **95**, 1998–2006 (2012).

[32]G. Catalan and J. F. Scott, "Physics and Applications of Bismuth Ferrite," *Adv. Mater.*, **21**, 2463–85 (2009).

[33]A. Loidl, S. Krohns, J. Hemberger, and P. Lunkenheimer, "Bananas Go Paraelectric," *J. Phys.:Condens. Matter*, **20**, 191001–3 (2008).

[34]J. F. Scott, "Ferroelectrics Go Bananas," *J. Phys.: Condens. Matter*, **20**, 021001–2 (2008).

[35]J. B. Batu, M. He, D. F. Zhang, X. L. Chen, and R. Dhanasekaran, "Enhancement of Ferroelectric Properties of $Na_{1/2}Bi_{1/2}TiO_3$–$BaTiO_3$ Single Crystals by Ce Doping," *Appl. Phys. Lett.*, **90**, 102901, 3pp (2007).

[36]L. Wang, X. L. Wang, and J. Shi, "Measurement and Estimation of Ferroelectric Hysteresis Loops," *Ferroelectrics*, **411**, 86–92 (2011).

[37]H. Yan, F. Inam, G. Viola, H. Ning, H. Zhang, Q. Jiang, T. Zeng, Z. Gao, and M. J. Reece, "The Contribution of Electrical Conductivity, Dielec-

tric Permittivity and Domain Switching in Ferroelectric Hysteresis Loops," *J. Adv. Dielectr.*, **1**, 107–18 (2011).

[38]P. A. Jha and A. K. Jha, "Influence of Processing Conditions on The Grain Growth and Electrical Properties of Barium Zirconate Titanate Ferroelectric Ceramics," *J. Alloy. Compd.*, **513**, 580–5 (2012).

[39]Y. S. Qiu, W. Li, Y. Liu, G. H. Liu, Y. Q. Wu, and N. Chen, "Phase Evolution and Room Temperature Ferroelectric and Magnetic Properties of Fe-Doped $BaTiO_3$ Ceramics," *Trans. Nonferrous Soc. China*, **20**, 1911–5 (2010).

[40]Y. F. Cui, Y. G. Zhao, L. B. Luo, J. J. Yang, H. Chang, M. H. Zhu, D. Xie, and T. L. Ren, "Dielectric, Magnetic, and Magnetoelectric Properties of La and Ti Co-Doped $BiFeO_3$," *Appl. Phys. Lett.*, **97** 2229904, 3pp (2010).

[41]H. Li, W. L. Yang, Y. Li, Q. X. Meng, and Z. X. Zhou, "Room-Temperature Magnetocapacitance in Fe-Doped $K_{0.5}Na_{0.5}Nb_{0.95}Ta_{0.05}O_3$ Ceramics," *Appl. Phys. Exp.*, **5**, 101501, 3pp (2012). □